Applied Catalysis B: Environmental 127 (2012) 342–350

Contents lists available at SciVerse ScienceDirect

Applied Catalysis B: Environmental

journal homepage: www.elsevier.com/locate/apcatb

Silica-encapsulated platinum catalysts for the low-temperature water-gas shift reaction

Yuan Wang, Yanping Zhai, Danny Pierre [1], Maria Flytzani-Stephanopoulos *

Department of Chemical and Biological Engineering, Tufts University, Medford, MA 02155, United States

ARTICLE INFO

Article history:
Received 17 May 2012
Received in revised form 21 August 2012
Accepted 30 August 2012
Available online 7 September 2012

Keywords:
Pt catalysts
Encapsulation
Reverse microemulsion
Water-gas shift reaction
Alkali promotion

ABSTRACT

Encapsulated platinum in the form of core–shell Pt@SiO_2 prepared by reverse microemulsion, can be rendered catalytically active for the low-temperature water-gas shift (WGS) reaction by the addition of alkali ions during the synthesis steps or by impregnation of the dried (uncalcined) core–shell materials. We report that positively charged platinum species, embedded throughout the silica shell and stabilized by the alkali ions are the active sites for the WGS reaction. Water dissociation and hydroxyl regeneration take place on the Na-promoted Pt–O_x sites. It is shown by cyclic CO-TPR experiments with intermittent ambient rehydration that the activity remains constant, and the onset temperature of the reaction is the same, ~150 °C, with cycling. The apparent activation energies for the WGS reaction in realistic fuel gas mixtures over the various encapsulated Pt-based catalysts evaluated here and those on other supports are all in the same range, 70 ± 5 kJ/mol. Hence any difference in the reaction rates between the open- and encapsulated-Pt catalysts is attributed to their different number of active sites accessible to the reactants. The Pt-Na@SiO_2 catalyst structures show remarkable stability with time-on-stream at 350 °C.

1. Introduction

The heterogeneously catalyzed water-gas shift (WGS) reaction is a key step in all carbon-based fuel processing aimed at producing and upgrading hydrogen gas streams [1]. For application to fuel cell systems, the WGS reaction catalysts must be non-pyrophoric, active over a wide temperature range, and stable during frequent shutdown-restart operation cycles. Noble metal-based catalysts have been widely investigated in recent years to meet these criteria for the low-temperature fuel cell applications [2–10].

The importance of noble metal and oxide support interaction for the WGS reaction has been discussed extensively in the literature [2–6]. Nanoscale ceria is the support of choice because of its high concentration of surface oxygen defects and hence, its ability to atomically disperse and stabilize active noble metal species [7–16]. Work done by Fu et al. documented the importance of such interaction between the noble metal (Au or Pt) and the oxygen of ceria, by showing that weakly-bound metallic gold or platinum nanoparticles on ceria are spectator species for the reaction, while the atomically dispersed [Au–O_x]–Ce or [Pt–O_x]–Ce species, strongly bound on ceria, are the active sites [7,15,16]. A great deal of research has been devoted to tailor the synthesis of the catalysts in order to maximize such strongly interacting species on supports. However, conventional techniques like deposition–precipitation or incipient wetness impregnation (IMP) cannot give the level of control required to systematically investigate the metal-support interaction and to maximize the metal-support interface. A novel synthesis approach which is demonstrable of nonmetallic Pt species interaction with ceria was reported by Yeung et al. [11]. Encapsulation of platinum nanoclusters inside a nanoscale shell of ceria was achieved by a reverse microemulsion technique. The resulting material showed excellent activity for the WGS reaction, presumably through atomically dispersed platinum in the ceria shell, while the undesired methanation reaction was suppressed by not exposing any metallic Pt sites.

Due to the rising price of rare-earth oxides, there is interest in finding alternative earth-abundant oxide supports for the noble metals or using promoters to achieve the kind of stable atomic dispersions afforded by ceria. It is also of fundamental interest to reproduce the type of active metal site on ceria on other supports, and the use of alkali and alkaline-earth ions as promoters has already been investigated for the WGS reaction catalysts [17–21]. In 1982, Amenomiya and Pleizier reported that addition of potassium rendered γ-alumina a high-temperature WGS reaction catalyst [22]. Later on, the study of alkali promotion was extended to Pt-based catalysts for the low-temperature WGS reaction with reducible or partially reducible oxide supports such as titania [18–20], zirconia [23], and ceria [24]. However, the interpretation of active site is complicated by the non-zero activity of

* Corresponding author.
E-mail address: maria.flytzani-stephanopoulos@tufts.edu (M. Flytzani-Stephanopoulos).
[1] Present Address: Cabot Corporation, Billerica, MA, United States.

0926-3373/$ – see front matter © 2012 Elsevier B.V. All rights reserved.
http://dx.doi.org/10.1016/j.apcatb.2012.08.038

Pt on these (alkali-free) supports. Most recently, Zhai et al. [21] reported that alkali ions can also significantly boost the catalytic performance of Pt catalysts on inert oxide supports, such as SiO_2 and Al_2O_3 for the low-temperature WGS reaction and proposed that alkali-stabilized Pt–$(OH)_x$ species are the active sites for the reaction. It was also proposed in that work that the same Pt–$(OH)_x$ species catalyze this reaction independent of the type of support. Understanding the alkali promotion would allow rational designs of new low-temperature WGS catalysts using very small amounts of Pt and a wide choice of a low-cost supports, e.g. silica or alumina for low-temperature shift applications.

Compared to other oxides, silica has been extensively used as a support due to its abundance and low-cost. Nanosized metal particles maximize the surface area exposed to the reactants leading to higher reactivity, but their thermal stability is limited. Imbedding the active phase improves the thermal stability of these nanostructures compared to conventional systems [25]. Kónya et al. [26] showed the stability of small Pt nanoparticles, protected by polymers, which they imbedded in the channels of SBA-15 by controlled hydrolysis of TEOS. The Pt particles located inside the channels were accessible to H_2 in chemisorption experiments. However, the silica encapsulation led to blocking part of the Pt and thus lowered its activity in toluene hydrogenation [27]. The stabilization of palladium in high temperature environments is rather difficult. The use of microemulsion has emerged as a particularly attractive technique to obtain the encapsulation of metal particles into silica oxide. Park et al. [28] prepared highly sintering-resistant Pd@SiO_2 catalysts by using two different silicon alkoxides as support precursors: TEOS and *n*-octadecyl trimethoxysilane as pore-forming agents. Small Pd cores of 4 nm were surrounded by a porous SiO_2 shell, approximately 10 nm thick. A Pd/SiO_2 with the same metal loading was also prepared by impregnation. After high-temperature calcination at 700 °C, only a slight increase in Pd particle size was found in the embedded catalyst, whereas the open-structured sample prepared by conventional impregnation showed significant agglomeration of the Pd particles.

In this work, we prepared a new, active and stable Pt-based WGS catalyst by combining two positive aspects: the promotion effect of catalytic activity by alkali ions [21] and the superior stability of the promoted metal species dispersed in core–shell structures. We further investigated whether the catalyst structure affects the intrinsic catalytic activity of alkali-modified Pt catalysts for the low-temperature WGS reaction. For this, we compared conventionally open-structured platinum catalysts with encapsulated platinum within a thin shell of silicon oxide (prepared via the reverse microemulsion technique). Na^+ ions were added at different steps in the preparation. Our aim in this work was not to advocate the core–shell structure as such for a practical WGS catalyst design; but rather to demonstrate that the promotion of Pt by Na ions could take place in such a structure, whether the alkali was added during the one-pot synthesis or in a second step after the formation of Pt@SiO2. Indeed, demonstrating the strong association of the Pt–O–Na species frees the designer from having to use CeO_2 or other reducible oxides to stabilize the Pt$(OH)_x$-active sites. The promotion is accompanied by improved stability of the active metal sites imparted by the confinement in the mesoporous silica shell.

Samples were characterized by scanning transmission electron microscopy (STEM), X-ray photoelectron spectroscopy (XPS), BET surface area, nitrogen porosimetry (NLDFT), and CO chemisorption. Temperature-programmed reduction (TPR) measurements were conducted using the reactant CO as the reductant. Catalytic activities of core–shell structured Pt@SiO_2 were evaluated for the WGS reaction under various gas conditions and compared with Pt catalysts prepared by conventional impregnation methods.

2. Experimental

2.1. Catalyst preparation

Platinum particles, encapsulated by a silica shell, were prepared by a reverse microemulsion method, following the approach described in ref. [29]. Accordingly, a certain amount of cationic surfactant, cetyltrimethylammonium bromide (CTAB, ≥98%, Sigma–Aldrich) was added to excess dried toluene at room temperature. An aqueous solution of $(NH_3)_4Pt(NO_3)_2$ was added drop wise to the surfactant–oil mixture to initiate the formation of micelles. After the stabilization of the micelle solution, 1 M NaOH or 50% NH_4OH aqueous solution was added to adjust the pH of the aqueous micelles in the bulk toluene and aged for 2 h followed by addition of hydrazine to reduce the platinum. To prepare a silica shell over the Pt particles, an amount of tetraethoxysilane (TEOS) was added, and the hydrolysis reaction between the basic solution and TEOS was allowed to proceed overnight. The final mixture was filtered and washed three times in hot ethanol and de-ionized water. The as-prepared samples were dried overnight at 100 °C and denoted as Pt-Na@SiO_2 (when NaOH was used to adjust the pH) and Pt@SiO_2 (when NH_4OH was used to adjust the pH). All dried samples were calcined at 400 °C at a heating rate of 2 °C/min in static air for 4 h.

A part of the dried Pt@SiO_2 was further impregnated to incipient wetness (IMP) final state with a $NaNO_3$ (Sigma–Aldrich) aqueous solution (0.3 M) followed by drying overnight at 100 °C. This is denoted as Na(IMP)-Pt@SiO2. Another part of Pt@SiO_2 was further impregnated with a small amount of cerium after precipitation of the silicon oxide. An amount of dissolved cerium(III) nitrate was added after TEOS to the basic solution, the pH of the solution being sufficiently basic (pH 10–11, controlled by ammonia) to precipitate cerium hydroxide within the pores of the silica shell. The final mixture was filtered, washed and dried overnight at 100 °C. This is denoted as Pt@SiO_2-CeO_2. All dried samples were calcined at 400 °C at a heating rate of 2 °C/min in static air for 4 h.

For comparison, supported Pt/SiO_2 was prepared by IMP. Typically, a commercial silica support (Sigma–Aldrich, fumed, S_{BET} = 243 m^2/g, V_p = 3 mL/g) was impregnated with an aqueous solution of the metal precursor, tetraammineplatinum(II) nitrate ($Pt(NH_3)_4(NO_3)_2$, Sigma–Aldrich, 99.995% trace metals basis). The volume of the solution was equal to the pore volume of the support. The wet powders were dried under vacuum at 100 °C overnight. A certain amount of Na was also added on the dried Pt/SiO_2 sample with an aqueous solution of $NaNO_3$ by the IMP method as well, denoted as Na(IMP)–Pt/SiO_2. All dried samples were calcined at 400 °C at a heating rate of 2 °C/min in static air for 4 h.

Selected, calcined Na-modified samples were washed by de-ionized water (D.I. water) to remove excess Na ions. The samples in powder form were suspended in sufficient amount of D.I. water and stirred at room temperature for 5 min. This was followed by filtering the suspension and drying the solid at 100 °C under vacuum overnight, further calcining it in static air at a heating rate of 2 °C/min and holding at 400 °C for 4 h.

To investigate the influence of the preparation methods, 0.8 at.% Pt/CeO_2 sample was prepared by deposition–precipitation (DP). Pre-made ceria support (prepared by Urea Gelation Coprecipitation method as in Ref. [8]) was suspended in D.I. water at room temperature. The desired amount of Pt precursor ($Pt(NH_3)_4((NO_3)_2)$ solution was added dropwise into a slurry of CeO_2 at pH 10, adjusted by 1 M ammonium carbonate ($(NH_4)_2CO_3$). After aging the mixture at room temperature for 1 h, the precipitate was filtered and washed with D.I. water at 60 °C three times, then dried in vacuum at 60 °C overnight, referred as Pt/CeO_2. All dried samples were

calcined in static air at a heating rate of 2 °C/min and held at 400 °C for 4 h.

2.2. Characterization

Bulk composition analysis of the catalysts was conducted in an inductively coupled plasma optical emission spectrometer (ICP-OES, EAG, NY). The BET surface area was measured by single-point N_2 adsorption and desorption cycles in a Micromeritics AutoChem II 2920 apparatus. The porosity was measured in a Quantachrome AutoSorb iQ instrument. A typical physisorption analysis started with degassing the sample in vacuum at 200 °C for 1 h. A classical helium void volume method was used. The volumetric adsorption measurements are performed at 77 K with multiple N_2 adsorption/desorption cycles over the desired P/P_0 ranges, providing the total pore volume and pore size distribution (calculation model: N_2 at 77 K on carbon, slit pore, NLDFT equilibrium model).

STEM analysis was performed in a Vacuum Generators HB603 STEM instrument equipped with an X-ray microprobe of 0.14 nm optimum resolution for energy dispersive X-ray spectroscopy (EDS). The sample powder was dispersed on a copper grid coated with a carbon film and elemental maps were obtained on a 128 × 128 data matrix.

XPS analysis was performed on a Kratos AXIS Ultra Imaging XPS with a resolution of 0.1 eV, used to determine the atomic ratios of the elements on the surface region and the oxidation state of platinum in selected samples. The powders were pressed on a double-sided adhesive copper tape for analysis. All measurements were carried out at room temperature without any pre-treatment. An Al Kα X-ray source was used and all binding energies were referenced to the Si_{2p} peak at 103.6 eV.

Pulse CO-chemisorption was carried out in the Micromeritics AutoChem II 2920 instrument equipped with a thermal conductivity detector (TCD). The Pt metal dispersion was measured by CO chemisorption at ambient temperature. Pretreatment was in 10%H_2–Ar at 350 °C for 2 h, followed by cooling down to room temperature in He. A linear CO adsorption on Pt (CO:Pt = 1:1) was assumed for the dispersion calculation [30].

CO temperature-programmed reduction (CO-TPR) was carried out in the Micromeritics AutoChem II 2920 instrument. Each component in the product gas stream was monitored by an on-line residual gas analyzer (SRS, RGA 200). The samples were heated at a rate of 5 °C/min from room temperature to 400 °C in 5%CO–He (20 mL/min). Cyclic CO-TPR was performed over selected samples with or without a vapor-flow (3%H_2O–He) treatment at room temperature between the cycles.

2.3. Catalytic activity tests

Steady-state WGS reaction tests to high conversions and steady-state kinetics measurements were conducted at atmospheric pressure in a packed-bed flow microreactor (A quartz tube with a porous quartz frit supporting the catalyst). The inlet and outlet gas streams were analyzed on-line by a gas chromatograph (HP-5890) equipped with TCD and using a Carbosphere (Alltech) packed column (80/100, 6 ft × 1/8 in.). The feed gas composition for the WGS tests was either product-free 2%CO–10%H_2O–He (70 mL/min, contact time = 0.09 g s/mL) or full-gas 11%CO–26%H_2O–26%H_2–7%CO_2–He (207 mL/min, contact time = 0.03 g s/mL), the latter used for the kinetics measurements with the reactor operated in a differential mode keeping the CO conversion below 15%; and also for isothermal stability tests.

3. Results and discussion

Table 1 shows the physical properties of the samples examined in this work. The commercial fumed silica support has a surface area of 210 m^2/g, while the core–shell structured samples all had comparably high surface areas and pore volume, indicating that the silica shell was highly porous and hence open to facile diffusion of the small reactant molecules of CO and H_2O to the "encapsulated" Pt sites. As shown in Table 1, Pt@SiO_2 prepared with ammonia has an especially high surface area of 400 m^2/g. However, the surface area dropped to ca. half this value in the Pt-Na@SiO_2 sample (198 m^2/g). These samples were further compared in terms of their pore volumes and pore-size distribution, as shown in Fig. 1. Both materials were mesoporous. Adding NaOH during the preparation lowered the pore volume considerably, i.e. the pore volume of Pt@SiO_2 and Pt-Na@SiO_2 was 0.55 mL/g and 0.18 mL/g, respectively. The corresponding pore size distribution changed from a narrow-sized one for the Pt@SiO_2 to a broader distribution for the Pt-Na@SiO_2 sample. As shown in Fig. 1, only a single peak at 19.9 Å (half pore width) was found in Pt@SiO_2 sample. A sharp peak at 23.8 Å was also observed in the Pt-Na@SiO_2 sample, and a broader size distribution between 30 and 80 Å. Overall, both samples have pores sizes of 4–5 nm in diameter, and these pores are adequate for reactant diffusion to the Pt sites in the 60 nm-thick silica shell. The Weisz–Prater criterion was used to estimate the influence of pore diffusion on the reaction rates [31]. Here the dimensionless Weisz–Prate number was much less than 0.3, hence diffusion limitations can be excluded [32].

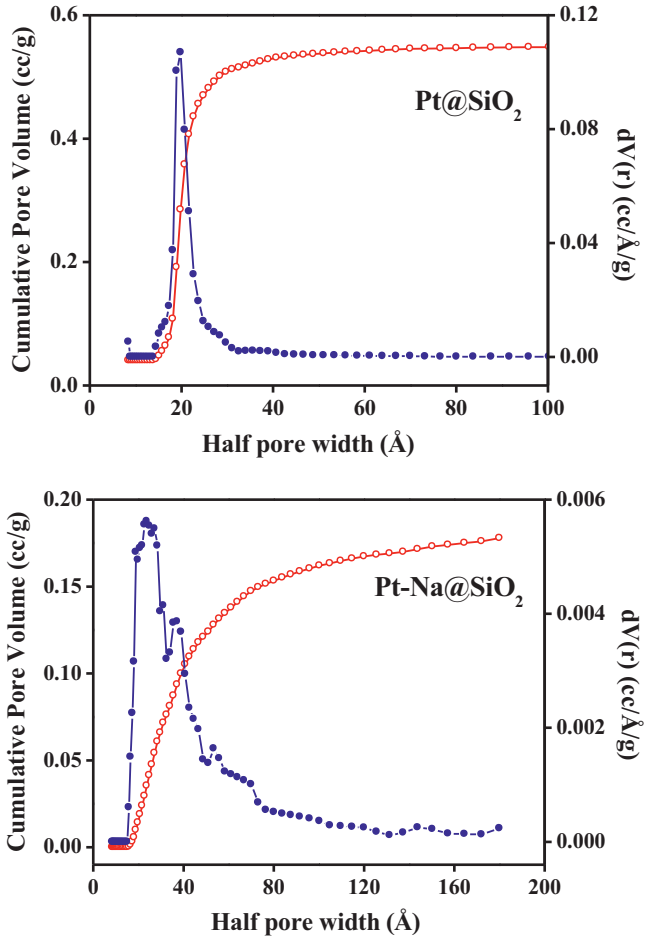

Fig. 1. Total pore volume and pore size distribution of as prepared Pt@SiO_2 and Pt-Na@SiO_2.

Table 1
Physical properties of the examined catalysts.

Catalysts	Bulk composition (at.%)		BET surface area[c] (m^2/g)	Pt particle size[d] (nm)	Pt dispersion[e] (%)
	Pt	Na			
SiO_2[a]	–	–	210	–	–
Na-SiO_2	–	3	203	–	–
Na-SiO_2 washed	–	–	203	–	–
Pt/SiO_2	1	–	187	4.8 ± 1.2	24
Na(IMP)-Pt/SiO_2	1	3	172	1.6 ± 0.4	71
Na(IMP)-Pt/SiO_2 washed	1	1.6	172	1.6 ± 0.4	93
Pt@SiO_2	1.1	–	400	2.8 ± 0.5 (6.5)	22
Na(IMP)-Pt@SiO_2	1.1	6.1	157	2.4 ± 0.8 (6.5)	5
Na(IMP)-Pt@SiO_2 washed	1.1	2.4	157	2.4 ± 0.8 (6.5)	8
Pt-Na@SiO_2	1	4.4	198	2.6 ± 0.5 (7.0)	6
Pt-Na@SiO_2 washed	1	2.7	198	2.6 ± 0.5 (7.0)	11
Pt@SiO_2-2%CeO_2	0.8	–	223	2.6 ± 0.5 (7.2)	–
Pt/CeO_2[b]	0.8	–	145	N.D.	–

[a] Sigma–Aldrich, fumed, S_{BET} = 243 m^2/g, V_p = 3 mL/g.
[b] Prepared by deposition–precipitation at pH 10; room temperature (ceria was pre-made by the UGC method as in Ref. [8]).
[c] Measured after calcination in air at 400 °C.
[d] Measured by TEM; particle size distribution of dispersed platinum throughout the shell was done from a survey of 50 particles; the platinum particle size at the core is shown in parenthesis.
[e] Calculated by CO chemisorption measurements at ambient temperature, assuming a linear CO adsorption on Pt [33].

Similarly drastic was the drop in surface area in the Ce-modified Pt@SiO_2 sample prepared as described above, and in the Na(IMP)-Pt@SiO_2 sample prepared by adding $NaNO_3$ solution in the pores of the dried Pt@SiO_2, followed by air calcination at 400 °C. Thus, the mesoporous silica material when wet-impregnated is apparently of low stability, and partially collapses upon calcination in air at 400 °C. Other protocols may be attempted to achieve impregnation without pore collapse, which would also eliminate or suppress the blocking of active platinum sites, but we did not pursue this line of research in the present work.

In recent work with Pt promoted by Na ions on open silica supports, it was reported that well-dispersed Pt–O_x species are formed and associate with Na ions, stabilizing a certain amount of the sodium around them, resisting a subsequent water-washing step [21]. Absent the Pt, all of Na washes out from the silica surface. A similar result was found here with the Na-modified encapsulated Pt@SiO_2 samples; i.e. some Na remained in the sample even after several washings. This is shown in Table 1 for both the Pt-Na@SiO_2 and Na(IMP)-Pt@SiO_2 samples. No Pt was found in the washing solution as checked by ICP. The residual alkali is then attributed to the interaction with the atomically dispersed Pt species, i.e. to strong Pt–O_x–Na interaction, resisting washing.

Around 1 at.% Pt was found by ICP in the samples prepared by the reverse microemulsion method and the average Pt particle size at the core measured by TEM was about the same, around 7 nm. The particle size can also be found in general by the metal dispersion calculated from chemisorption measurements. Atomically-dispersed Pt–O_x species are reported to be the active sites for the WGS reaction on ceria [7,15], and for the alkali-promoted Pt on inert, open supports [21]. Here, because of the core–shell structure, the accessibility of these sites is at issue. CO chemisorption at room temperature was used to address the accessibility and measure the dispersion of Pt species in the encapsulated samples. The Pt dispersion thus calculated was 22% in the Pt@SiO_2 sample but a lower value of 5–6% was found for the Pt-Na@SiO_2 and Na(IMP)-Pt@SiO_2 samples, assuming a linear CO adsorption on Pt in all cases [33]. With higher alkali loading, the nominal Pt dispersion was further decreased. One possibility with the high loading of alkali is that some part of the platinum was fully covered, hence inaccessible to CO. Indeed, the Pt dispersion increased after the water washing treatment due to the removal of excess Na and exposure of more Pt sites to CO, as Table 1 shows. Another reason for the different dispersion is that the strength of CO adsorption on the Na-promoted Pt was different. Weaker CO binding has been reported for alkali-modified Pt/Al_2O_3, with the mode of CO–Pt adsorption partially changed from linear to bridged adsorption [34]. Thus, it is hard to estimate the Pt dispersion in these Na-modified samples by CO chemisorption, because the assumption of CO: Pt = 1:1 may not hold true for the part of Pt that is associated with Na ions. Moreover, the estimated dispersion is distorted also by the presence of platinum as large nanoparticles at the core of these structures; and by the inaccessible (blocked off) platinum. Since we do not know the exact amount of Pt in these locations, we cannot use the chemisorption measurements to compare to the TEM results. And TEM, in turn, is not good enough to image sub-nm clusters and atoms. Atomic-resolution STEM imaging is preferred, if available.

The STEM image in Fig. 2 confirms the encapsulation of platinum nanoclusters within the silicon oxide shell of the Pt-Na@SiO_2 sample. The platinum cores are on the order of 7–10 nm with 60 nm-thick silica shells. The elemental maps obtained from the EDS analysis of Pt-Na@SiO_2 in Fig. 3 not only show a high

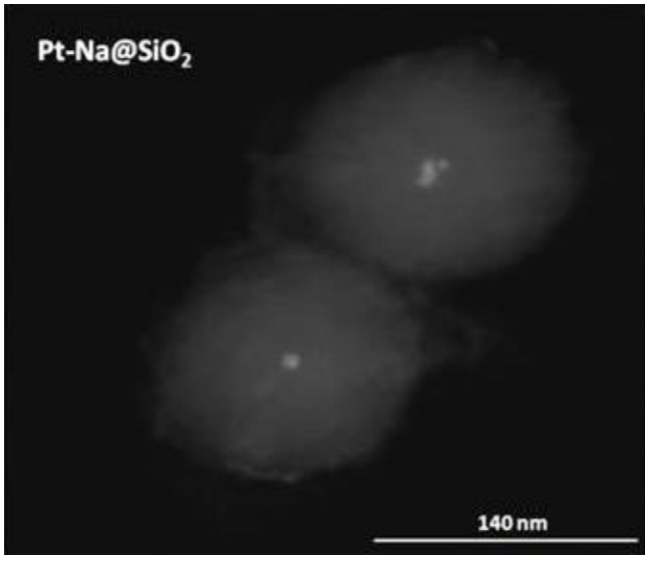

Fig. 2. STEM image of the as prepared Pt-Na@SiO_2 sample; after air calcination at 400 °C.

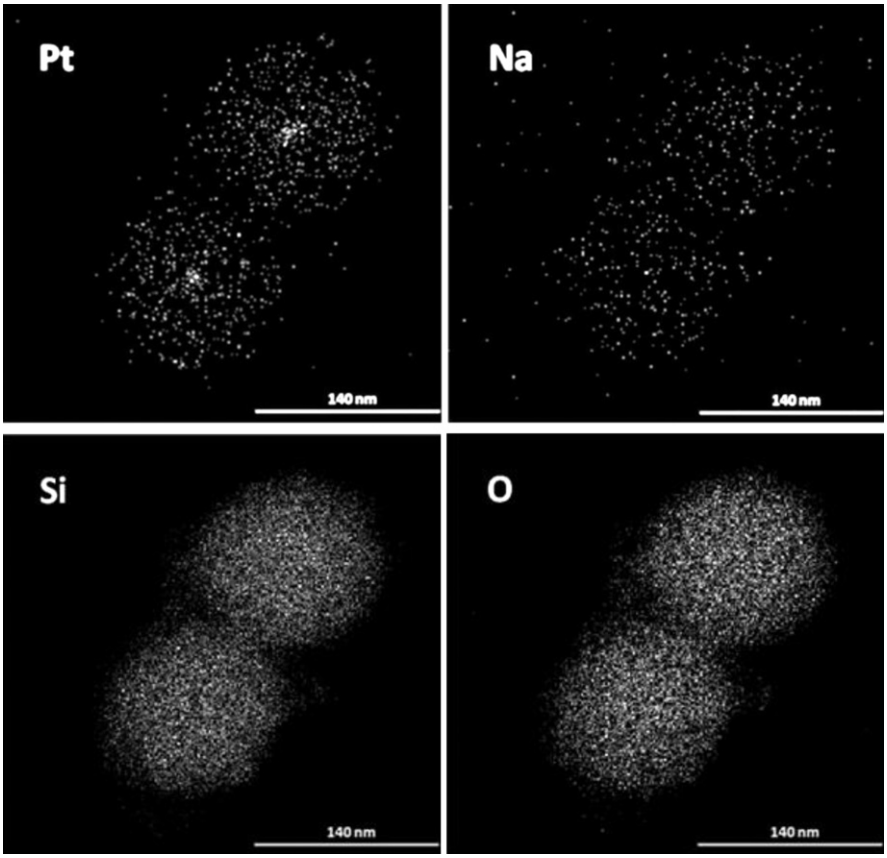

Fig. 3. Elemental maps of (a) Pt (b) Na (c) Si (d) O of the Pt-Na@SiO_2 sample shown in Fig. 2.

concentration of platinum at the center (core) of the particles, but also the existence of small platinum clusters (<1 nm) embedded throughout the pores of the silica shell. To further investigate the metal distribution in this core–shell structured sample, elemental linescans were performed on one silicon dioxide spherical shell. In this cross sectional scan, as shown in Fig. 4, platinum is found distributed throughout the silica shell, not only at the core of the sphere. This finding supports the argument that the platinum species are embedded in the silica shell. This also explains why residual Na was found in the well-washed Pt-Na@SiO_2, since atomically dispersed Pt species stabilize and retain Na ions, and only the unassociated sodium washes out [21]. Metal particle deposition in the pores of a highly mesoporous material is not uncommon in microemulsion techniques. Calderone et al. [35] found that other than being encapsulated by the silica at the core during the silica coating, the Pt species could also be dispersed throughout the shell as demonstrated by TEM images. Thus, it is not surprising to see the dispersed Pt clusters in the 4–5 nm-diameter pores of the materials prepared in this work.

Overall, it is clear that in the core–shell structured Pt samples, only a minority of the Pt species will exist as clusters and atoms in the pores of the silica shell and accessible to CO. If reaction is

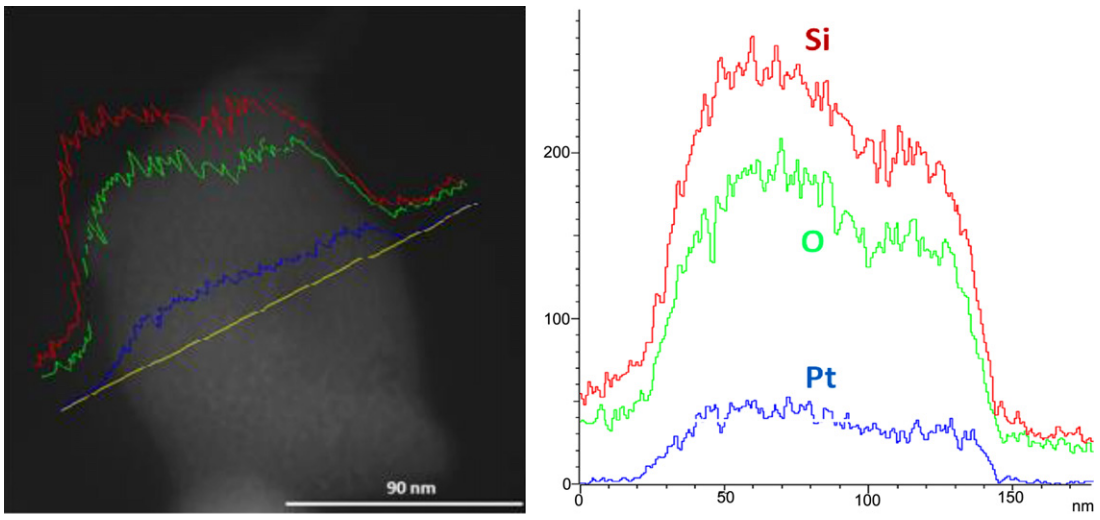

Fig. 4. Elemental linescans of as prepared Pt@SiO_2; after air calcination at 400 °C.

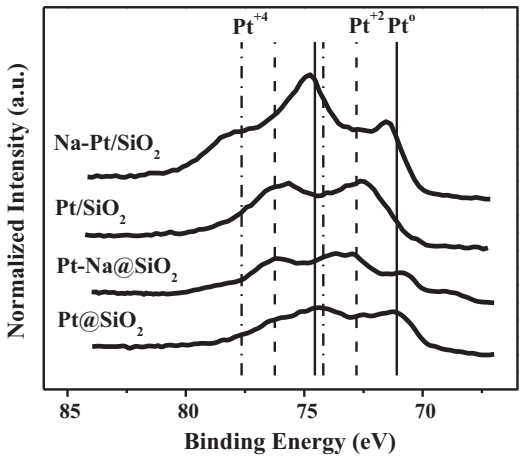

Fig. 5. XP spectra of Pt_{4f} in $Pt@SiO_2$ and Pt/SiO_2 samples with or without Na-modification.

observed, this will be due to the presence of this phase and not the big platinum particles at the core or elsewhere in the mesoporous silica shell. Hence these core–shell structures can be used to check whether a reaction known to occur on either the metallic or the nonmetallic state of platinum takes place. For example, in Ref. [11], the $Pt@CeO_2$ core–shell catalyst was excellent for the WGS reaction, but inactive for the methanation reaction, the latter catalyzed by metallic Pt sites.

The small Pt clusters dispersed throughout the silica shell are highly interesting. In recent work, it was reported that well-dispersed Pt species can associate with Na ions, and the Na-modified Pt is positively charged [18,21]. XPS measurements were conducted to check the oxidation states of Pt in the samples examined and tested in this work. Initial- and final-state effects have been reported to shift the binding energy of Pt clusters on the support. Generally, final-state effects cause a positive shift of the binding energy of metallic nanoparticles as their size is decreased [33], but below a certain cluster size (~2 nm), initial-state effects prevail [36], which is determined principally by the electronegativities of the atoms involved. Fig. 5 shows XP spectra for Pt_{4f}, the binding energy assignments for Pt^0 at 71.1 and 74.5 eV, Pt^{2+} at 72.8 and 76.2 eV, and Pt^{4+} at 74.2 and 77.6 eV, respectively [37]. With the addition of Na ions, the peaks shifted to higher binding energies. The observed positive shift (by 1.7 eV) shows a clear increase of the fraction of oxidized Pt species in the encapsulated $Pt\text{-}Na@SiO_2$ sample. The same trend was observed in the open-structured material $Na(IMP)–Pt/SiO_2$ [21]. For the open $Na(IMP)–Pt/SiO_2$ sample, the positive energy shift was attributed to the smaller Pt cluster sizes and the electron deficiency of Pt species in the presence of $Na–O_x$ species [21].

It is also seen in Fig. 5 that the intensity of the Pt in the sample of $Na–Pt/SiO_2$ is higher than that of Pt/SiO_2 for the same amount of Pt loading. The difference of the Pt intensities is due to the difference of Pt surface concentration in the two samples. For the open $Na–Pt/SiO_2$ sample, most of the Pt species are on the silica pore surface. However, some of the Pt atoms or clusters in $Pt@SiO_2$ are totally blocked by the silica shell, at a depth higher than the escape depth of the electrons excited by the X-ray beam. Thus, the deeper located platinum species are inaccessible to the beam. A lower amount of CO adsorption also indicated the partial inaccessibility of the Pt species in the $Pt@SiO_2$ sample. Addition of Na to the core–shell structured sample caused pore collapse, which resulted to further blocking of platinum sites and lowered the Pt intensity in XPS, as well as the metal dispersion measured by CO chemisorption in the Na-containing $Pt@SiO_2$ samples.

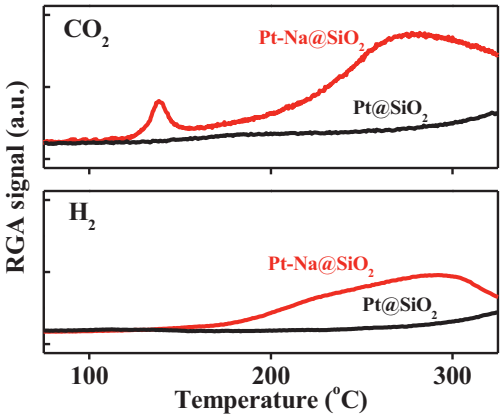

Fig. 6. CO-TPR test of $Pt@SiO_2$ and $Pt\text{-}Na@SiO_2$ catalysts.

CO-TPR was used here to identify reducible surface oxygen species and probe the onset of the WGS reaction by activation of the surface hydroxyls to produce CO_2 and H_2. As shown in Fig. 6, there is no CO_2 or H_2 production over the Na-free $Pt@SiO_2$ sample till 300 °C. With Na in the sample, $Pt\text{-}Na@SiO_2$ showed CO_2 and H_2 production from ~150 °C. The same was true for the conventionally prepared $Na–Pt/SiO_2$ sample, consistent with what has been reported before [21]. Hence, the addition of Na introduces both reducible surface oxygen species and active surface hydroxyl groups to the dispersed Pt species. The $Pt–O_x(OH)–Na$ species shifts the onset of surface reduction and as shown below, the WGS reaction, to lower temperatures.

In order to evaluate the reversibility of the hydroxyl groups on $Pt\text{-}Na@SiO_2$ cyclic CO-TPR tests were conducted. If a second cycle of CO-TPR was carried out without any treatment after the first cycle, negligible CO_2 and H_2 productions were detected, as shown in Fig. 7, which means most of the reducible species had been consumed and surface OH groups were depleted during the first cycle. If a rehydration treatment was introduced between the two cycles, with helium saturated with water vapor ($3\%H_2O–He$) flowing through the reactor at room temperature for an hour, full recovery of the —OH groups was found, as shown in Fig. 8 by the full recovery of H_2 production along with the CO_2.

During the CO-TPR experiments, the evolution of a small CO_2 peak at ~130 °C is attributed to the reaction between CO and active surface oxygen, so this is the "dry" CO_2 production without any evolution of H_2. Afterwards, CO_2 and H_2 were produced simultaneously, from the reaction between CO and active hydroxyl groups. After the first cycle of CO-TPR test, we did an in situ water vapor

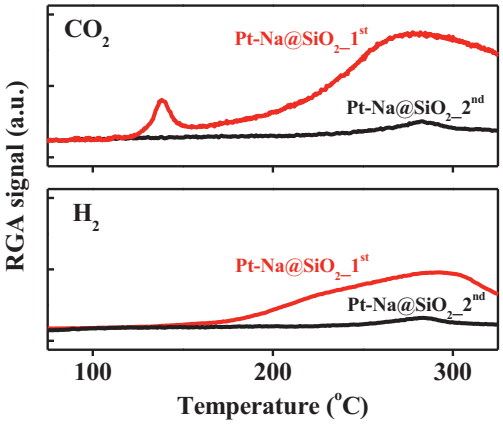

Fig. 7. CO-TPR tests of $Pt\text{-}Na@SiO_2$ catalyst in two consecutive cycles with no intermittent rehydration.

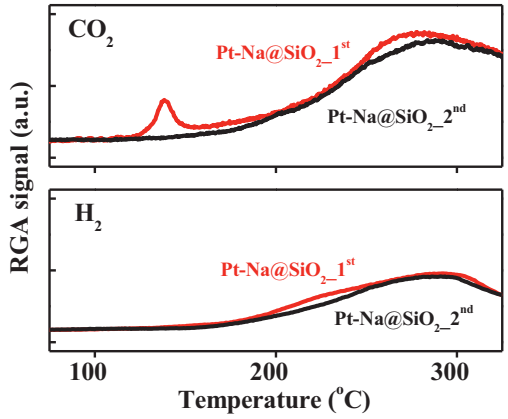

Fig. 8. Cyclic CO-TPR tests of Pt-Na@SiO_2 catalyst with intermittent rehydration at room temperature.

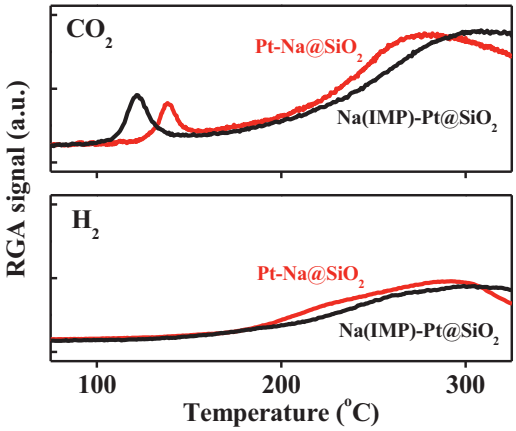

Fig. 10. CO-TPR test of Pt-Na@SiO_2 and Na(IMP)-Pt@SiO_2 catalysts.

treatment of the sample, which exposed the sample to 3% H_2O (balanced with He), but to no air (or oxygen). Rehydration, but no reoxidation, takes place on the Na-promoted Pt–O_x sites, so the –OH species are regenerated, but not the surface oxygen species. Thus the first "dry" CO_2 peak disappears in the cyclic CO-TPR tests, as shown in the second CO-TPR cycles of Figs. 7 and 8.

These cyclic CO-TPR tests demonstrate that the activation of water and the regeneration of OH groups take place on the Na-promoted Pt sites at low temperatures (~120 °C). This is the feature that renders the Pt–O_x(OH)–Na cluster active for the low-temperature WGS reaction, as also shown for the open Na–Pt/SiO_2 supports in [21]. The full recovery of surface hydroxyl groups on Pt-Na@SiO_2 during subsequent water treatment also indicates that no surface carbonate was formed on the sample in the CO-TPR tests. Otherwise, the active sites would be blocked by carbonates, since a room temperature water vapor treatment cannot decompose them.

Similar to the CO-TPR data, the activity plots, in Fig. 9, show that sodium addition has the same promotion effect on the activity of the encapsulated platinum catalyst for the WGS reaction as for the open Pt/SiO_2 catalyst. The Na-free samples, Pt@SiO_2 and Pt/SiO_2, show no activity for the reaction up to 300 °C, while the Na-containing samples are active, perhaps as active in terms of TOF as the Pt/CeO_2 sample, shown in Fig. 9. As explained by the CO chemisorption results, the open Pt-Na/SiO_2 samples have a larger number of active sites available than the core–shell Pt-Na@SiO_2 samples, which accounts for the better total activity of the former. However, the specific (intrinsic) activity may be the same, as indicated by the same light-off temperature (100 °C) and the same apparent activation energies (see below). Also Pt-Na@SiO_2 may have some active sites that are less accessible to the gases. A similar conclusion was made for Pt particles located inside the channels of SBA-15 which were partially blocked by silica coverage that lowered their activity for toluene hydrogenation [27]. Therefore, the activity difference must be due to the difference in the population and accessibility of the active sites.

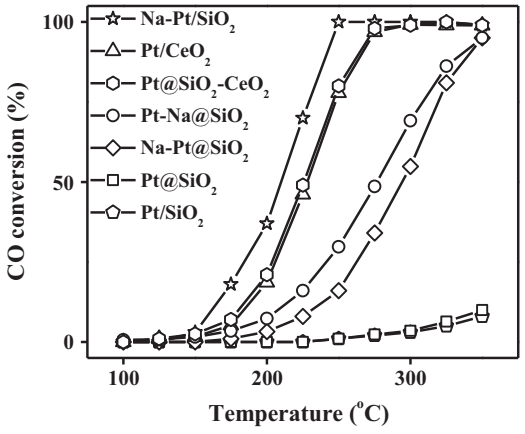

Fig. 9. CO conversion profiles in steady-state tests of WGS reaction over Pt@SiO_2, Pt/SiO_2 and Pt/CeO_2 catalysts (2%CO–10%H_2O–He, 70 mL/min, contact time = 0.09 g s/mL).

Without sodium, Pt@SiO_2 is not active for the WGS reaction due to the lack of surface oxygen and hydroxyl groups. For the Na(IMP)-Pt@SiO_2 sample, CO-TPR showed that Na introduced the active OH groups in the proximity of the Pt with which they could interact and form stable Pt-O_x(OH)–Na species. As shown in Fig. 10, the CO activated the OH and produced CO_2 and H_2 similar to the Pt-Na@SiO_2 sample. In turn, Na(IMP)-Pt@SiO_2 showed similar activity as Pt-Na@SiO_2 in the steady-state WGS reaction tests, see Fig. 9. This series of experiments also shows that the atomically dispersed minority phase of Pt in the core–shell preparations is there (in the shell) even when no Na was used in the preparation. These sites are simply not stabilized and not activated unless Na is added even in a post-preparation step.

A single-pot microemulsion procedure was adapted to prepare Pt@SiO_2–2%CeO_2 sample. Unlike the previous ones, where NaOH or $NaNO_3$ additive was used, this material had no sodium and a relatively high surface area of 223 m^2/g. The addition of cerium salt took place toward the end of the synthesis, and this coupled with slow precipitation, allowed for uniform cerium oxide distribution throughout the silica shell. For comparison, a Pt/CeO_2 sample made by deposition–precipitation was also tested here. This sample had identical activity to the Pt@SiO_2–2%CeO_2 sample containing only 2 at.% ceria. A small amount of ceria additive is thus sufficient to fully interact with and stabilize the dispersed platinum species in the silica shell and therefore yield a very active material to catalyze the WGS reaction. It is also clear that sodium promotion of Pt is similar to that of CeO_2, the sodium addition being as effective as addition of ceria in promoting Pt for the WGS reaction. This has significant implications for practical catalyst design.

The Na-promotion effect on the WGS reaction activity over the Pt-based catalysts is further confirmed in activity tests conducted in the full reformate gas mixture, as depicted in Fig. 11. Comparing the apparent activation energy (E_{app}) of the WGS reaction over the different samples, it is clear that the E_{app} over all the Pt-based samples falls into the same range, 70 ± 5 kJ/mol. As discussed in Ref. [21], this demonstrates that the Na-promotion is independent of the support structure and type. Na ions stabilize the Pt ions and facilitate the regeneration of the active OH groups, continuously providing OH to complete the reaction pathway. These OH groups

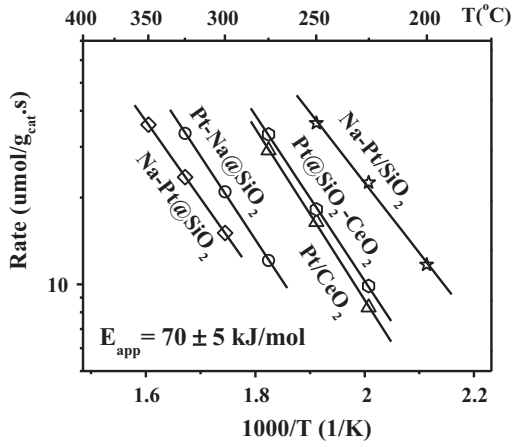

Fig. 11. WGS reaction rate and apparent activation energy over Pt@SiO_2 and Pt/SiO_2 series and Pt/CeO_2 catalysts.

are not present on alkali-free Pt/SiO_2 or Pt@SiO_2 surfaces, but they are on ceria. Hence the Pt–O_x(OH)–Ce and the Pt–O_x(OH)–Na clusters are analogs. The same apparent activation energy over CeO_2- or SiO_2-supported Pt catalysts gives further support to this conclusion, i.e. the Pt–O_x(OH)–M species is the active site, irrespective of what M is chosen. It will be important mechanistically and useful practically to add other such ligands and extend this finding to other additives and supports.

The long-term stability of Pt-Na@SiO_2 was evaluated for the WGS reaction as shown in Fig. 12. This experiment aimed at testing whether the Na-promoted Pt@SiO_2 catalysts can maintain their good activity at temperatures as high as 350 °C for up to 60 h in the full reformate gas stream. It was not meant as a test of any shifts in the light-off temperature. From the CO-TPR and product-free WGS steady tests (Fig. 9), the first CO_2 and H_2 measurable production was observed at ~150 °C, so under those test conditions there was close to zero activity of the Pt-Na@SiO_2 catalyst at 100 °C. Moreover, the sample was heated to 350 °C from RT or 100 °C at a heating rate of 10 °C/min, but the GC sampled the outlet gas every 7 min. Thus, there was no steady-state attained between 150 and 200 °C. To get the information for the low-temperature activity, steady-state test data were collected every 50 °C from RT to 350 °C in the product-free reaction gas, see Fig. 9. Also the production of CO_2 and H_2 was monitored on-line by mass spectrometry in the CO-TPR tests, which aimed at light-off temperature examination and which are more sensitive to the low-concentration CO_2 production. These tests show no effect of cycling. In regards to attaining thermodynamic equilibrium, the tests in Fig. 12 were intentionally run at very short contact times (0.03 g s/mL), so the long-term stability

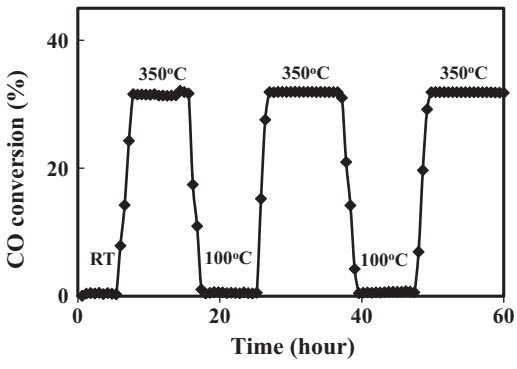

Fig. 12. Stability test over Pt-Na@SiO_2 catalyst at 350 °C (11%CO–26%H_2O–26%H_2–7%CO_2–He, 207 mL/min, contact time = 0.03 g s/mL).

of Pt-Na@SiO_2 could be evaluated for the WGS reaction far from equilibrium in the full reformate gas stream at 350 °C for about 60 h. After several shutdown-startup operation cycles, this catalyst maintained its activity throughout the test. The equilibrium CO conversion at 350 °C for this gas mixture is >99%. Since the operation is far from equilibrium, the ca. 35% CO conversion on the Pt-Na@SiO_2 catalyst should be attributed to all the accessible Pt sites in this sample. Hence, we conclude that the encapsulated Pt catalyst has excellent stability in a realistic fuel gas mixture and can be used even at higher temperatures than those intended for practical, low-temperature shift catalysts. During the long-term stability test of Pt-Na@SiO_2, the gas flow was not interrupted during the shutdown operation. The well maintained activity for 60 h further supports the previous discussion about exclusion of carbonate formation on the sample surface. Otherwise, we would see a gradual deactivation of the sample. Long-term stability with time-on-stream is an important property if the catalysts are to be developed for commercial WGS applications.

4. Conclusions

In this work we have investigated the catalytic activity and stability of encapsulated platinum catalysts for the WGS reaction. Platinum clusters and atoms are highly dispersed throughout the silica shell and well maintained during the reaction. The Na-free Pt@SiO_2 is not active for the reaction up to 300 °C, while addition of Na, either in the synthesis step or by impregnation of the core–shell sample, renders the corresponding Pt-Na@SiO_2 or Na(IMP)-Pt@SiO_2 a very active catalyst for the WGS reaction.

The active Pt–O_x(OH)–Na species in the silica shell of the Pt-Na@SiO_2 and Na(IMP)-Pt@SiO_2 catalysts dissociate water and regenerate surface hydroxyl groups. Incorporation of sodium on these encapsulated Pt catalysts enhances their catalytic activity to equivalent levels of Na-promoted, open Pt/SiO_2 catalysts. An oxidized Pt–O_x(OH) species associated with alkali ions or cerium ions is concluded to be the active site for the low-temperature WGS reaction, which can be manifested on any support. The overall activity difference is due to differences in the population and accessibility of the active sites.

Acknowledgments

We acknowledge the financial support of this work from the U.S. Department of Energy/Basic Energy Sciences (grant no. DE-FG02-05ER15730). D.P. acknowledges the National Science Foundation (NIRT grant no. 0304515) for partial support of his thesis work. Y.W. and Y.Z. acknowledge the support from AFOSR (MURI) grant no. FA9550-08-1-0309. Y.W. thanks Dr. Herui Dou (Y. Roman's group, MIT) for his assistance with the porosity measurements of the core-shell samples.

References

[1] W. Ruettinger, O. Ilinich, R.J. Farrauto, Journal of Power Sources 118 (2003) 61–65.
[2] D. Tibiletti, A. Goguet, F.C. Meunier, J.P. Breen, R. Burch, Chemical Communications (2004) 1636–1637.
[3] K.G. Azzam, I.V. Babich, K. Seshan, L. Lefferts, Journal of Catalysis 251 (2007) 163–171.
[4] Y. Sato, K. Terada, S. Hasegawa, T. Miyao, S. Naito, Applied Catalysis A: General 296 (2005) 80–89.
[5] H. Iida, A. Igarashi, Applied Catalysis A: General 303 (2006) 48–55.
[6] Y. Bi, W. Zhang, H. Xu, W. Li, Catalysis Letters 119 (2007) 126–133.
[7] Q. Fu, H. Saltsburg, M. Flytzani-Stephanopoulos, Science 301 (2003) 935–938.
[8] D. Pierre, W. Deng, M. Flytzani-Stephanopoulos, Topics in Catalysis 46 (2007) 363–373.
[9] W. Deng, M. Flytzani-Stephanopoulos, Angewandte Chemie International Edition 45 (2006) 2285–2289.

[10] C.M.Y. Yeung, F. Meunier, R. Burch, D. Thompsett, S.C. Tsang, Journal of Physical Chemistry B 110 (2006) 8540–8543.
[11] C.M.Y. Yeung, K.M.K. Yu, Q.J. Fu, D. Thompsett, M.I. Petch, S.C. Tsang, Journal of the American Chemical Society 127 (2005) 18010–18011.
[12] M. Hatanaka, N. Takahashi, N. Takahashi, T. Tanabe, Y. Nagai, A. Suda, H. Shinjoh, Journal of Catalysis 266 (2009) 182–190.
[13] J.M. Zalc, V. Sokolovskii, D.G. Loffler, Journal of Catalysis 206 (2002) 169–171.
[14] X. Liu, W. Ruettinger, X. Xu, R. Farrauto, Applied Catalysis B: Environmental 56 (2005) 69–75.
[15] Q. Fu, W. Deng, H. Saltsburg, M. Flytzani-Stephanopoulos, Applied Catalysis B: Environmental 56 (2005) 57–68.
[16] W. Deng, A.I. Frenkel, R. Si, M. Flytzani-Stephanopoulos, The Journal of Physical Chemistry C 112 (2008) 12834–12840.
[17] A. Hagemeyer, R.E., Carhart, K., Yaccato, A., Lesik, C.J. Brooks, United States Patent Application 20040175325 (2004).
[18] X. Zhu, M. Shen, L.L. Lobban, R.G. Mallinson, Journal of Catalysis 278 (2011) 123–132.
[19] P. Panagiotopoulou, D.I. Kondarides, Applied Catalysis B: Environmental 101 (2011) 738–746.
[20] P. Panagiotopoulou, D.I. Kondarides, Journal of Catalysis 267 (2009) 57–66.
[21] Y. Zhai, D. Pierre, R. Si, W. Deng, P. Ferrin, A.U. Nilekar, G. Peng, J.A. Herron, D.C. Bell, H. Saltsburg, M. Mavrikakis, M. Flytzani-Stephanopoulos, Science 329 (2010) 1633–1636.
[22] Y. Amenomiya, G. Pleizier, Journal of Catalysis 76 (1982) 345–353.
[23] J.M. Pigos, C.J. Brooks, G. Jacobs, B.H. Davis, Applied Catalysis A: General 319 (2007) 47–57.
[24] H. Evin, G. Jacobs, J. Ruiz-Martinez, U. Graham, A. Dozier, G. Thomas, B. Davis, Catalysis Letters 122 (2008) 9–19.
[25] L. De|Rogatis, M. Cargnello, V. Gombac, B. Lorenzut, T. Montini, P. Fornasiero, ChemSusChem 3 (2010) 24–42.
[26] Z. Kónya, V.F. Puntes, I. Kiricsi, J. Zhu, A.P. Alivisatos, G.A. Somorjai, Nano Letters 2 (2002) 907–910.
[27] S. Chytil, W.R. Glomm, E. Vollebekk, H. Bergem, J. Walmsley, J. Sjöblom, E.A. Blekkan, Microporous and Mesoporous Materials 86 (2005) 198–206.
[28] J.-N. Park, A.J. Forman, W. Tang, J. Cheng, Y.-S. Hu, H. Lin, E.W. McFarland, Small 4 (2008) 1694–1697.
[29] K.M.K. Yu, C.M.Y. Yeung, D. Thompsett, S.C. Tsang, Journal of Physical Chemistry B 107 (2003) 4515–4526.
[30] S. Derrouiche, P. Gravejat, B. Bassou, D. Bianchi, Applied Surface Science 253 (2007) 5894–5898.
[31] P.B. Weisz, C.D. Prater, V.I.K.W.G. Frankenburg, E.K. Rideal, Advances in Catalysis 6 (1954) 143–196.
[32] M.A. Vannice, Kinetics of Catalytic Reactions, Springer Science + Business Media, New York, 2005.
[33] C.R. Henry, Surface Science Reports 31 (1998) 231–325.
[34] H. Tanaka, M. Kuriyama, Y. Ishida, S.-i. Ito, T. Kubota, T. Miyao, S. Naito, K. Tomishige, K. Kunimori, Applied Catalysis A: General 343 (2008) 125–133.
[35] V. Calderone, J. Schütz-Widoniak, G. Bezemer, G. Bakker, C. Steurs, A. Philipse, Catalysis Letters 137 (2010) 132–140.
[36] J. Radnik, C. Mohr, P. Claus, Physical Chemistry Chemical Physics 5 (2003) 172–177.
[37] National Institute of Standards and Technology X-ray Photoelectron Spectroscopy Database Version 3.5, http://srdata.nist.gov/xps/, 2003.